Cement and Concrete Research 38 (2008) 1038–1048

Contents lists available at ScienceDirect

Cement and Concrete Research

journal homepage: http://ees.elsevier.com/CEMCON/default.asp

Heterogeneous porosity distribution in Portland cement exposed to CO_2-rich fluids

Gaëtan Rimmelé [a,*], Véronique Barlet-Gouédard [a], Olivier Porcherie [a], Bruno Goffé [b], Fabrice Brunet [b]

[a] Schlumberger Riboud Product Center, Well Integrity Technologies, 1 rue Henri Becquerel, BP 202, 92142, Clamart, France
[b] Ecole normale supérieure, CNRS, Laboratoire de Géologie, 24 rue Lhomond, 75005, Paris, France

ARTICLE INFO

Article history:
Received 26 October 2007
Accepted 30 March 2008

Keywords:
Wellbore integrity
CO_2 storage
Portland cement
Carbonation
Mercury intrusion porosimetry
Scanning electron microscopy
Porosity profiles

ABSTRACT

Efficient and safe storage of injected supercritical carbon dioxide (CO_2) underground is now one potential solution for reducing CO_2 emissions in the atmosphere. Preventing any CO_2 leakage through a wellbore annulus after injection is a key to maintaining long-term wellbore integrity. Most wells in depleted oil and gas fields may be re-used to inject CO_2. These wells were mostly cemented with conventional Portland cement. It is thus crucial to study how such cement behaves at depth in CO_2-rich fluids.

Set cement samples are exposed to CO_2 fluids under pressure and temperature to simulate downhole conditions. The degraded cement exhibits significant mineralogical changes and heterogeneous porosity distribution. The bulk porosity evolution, as well as local porosity gradients through the samples, is quantified using combined mercury porosimetry and back-scattered electron image analysis. Both techniques show an initial sealing stage related to calcium carbonate precipitation plugging the porosity, followed by a dissolution stage marked by a significant increase of porosity.

1. Introduction

Injection of carbon dioxide (CO_2) underground is a common technique for enhanced oil and gas recovery operations [1–4]. Such applications concern very short time-scales compared with the needs of efficient and safe storage of supercritical CO_2 in geological reservoirs for hundreds to thousands years. One major long-term risk is CO_2 leakage through a wellbore annulus. The long-term wellbore integrity of the cement sheath when exposed to CO_2 is therefore a key requirement.

Three main types of geological reservoirs have sufficient capacity to store captured CO_2: depleted oil and gas reservoirs, deep saline aquifers and unminable coal beds [5]. In depleted oil and gas fields, most wells that may be re-used to inject CO_2 were cemented with conventional Portland cement. Therefore, it is crucial to study how such cement behaves at depth in the presence of CO_2-rich fluids.

Up to now, most of the experimental work dedicated to study natural carbonation of cementitious material for building industry is done at atmospheric pressure [6–8]. In contrast, for this study, we want to simulate a CO_2-rich environment under downhole conditions. For this purpose, we built laboratory equipment and developed a standard CO_2-testing procedure for the qualification and comparison of the CO_2 resistance of different cements [9,10]. CO_2 diffuses rapidly through Portland cement and significantly modifies its chemical and physical properties; therefore, these changes can be monitored with microscopic characterization methods.

This paper focuses on the porous-network evolution of Portland-cement samples placed in the CO_2-testing equipment and exposed to wet supercritical CO_2 and CO_2-saturated water at downhole pressure and temperature conditions. After presenting the experimental equipment and procedure, some mineralogical features of the cement samples are described, as they are exposed to CO_2 at several durations through the six months of the experiment. The CO_2-alteration pattern of Portland cement is microscopically characterized. Then, the evolution of cement porosity over time is discussed, based on results obtained with two different techniques: (1) mercury intrusion porosimetry (MIP) providing information on the global porosity of cement and pore-entrance size distribution; (2) scanning electron microscope (SEM) image analysis used to quantify local porosity gradients commonly observed throughout the cement samples exposed to CO_2 fluids.

2. Experimental set-up and run procedure

Portland cement samples (Class G well cement [11], slurry density = 1.89 g/cm^3) used for CO_2-laboratory experiments are prepared according to ISO/API Specifications 10, section 5 using fresh water. Cement slurry is cured in cubic molds for 72 h at 207 bars and 90 °C, following the ISO/API standard procedures to simulate the setting of the cement under wellbore downhole conditions. Cylindrical samples of about 1.25-cm diameter are obtained by coring the set

* Corresponding author. Tel.: +33 1 45 37 29 07; fax: +33 1 45 37 25 13.
E-mail address: grimmele@clamart.oilfield.slb.com (G. Rimmelé).

0008-8846/$ – see front matter © 2008 Elsevier Ltd. All rights reserved.
doi:10.1016/j.cemconres.2008.03.022

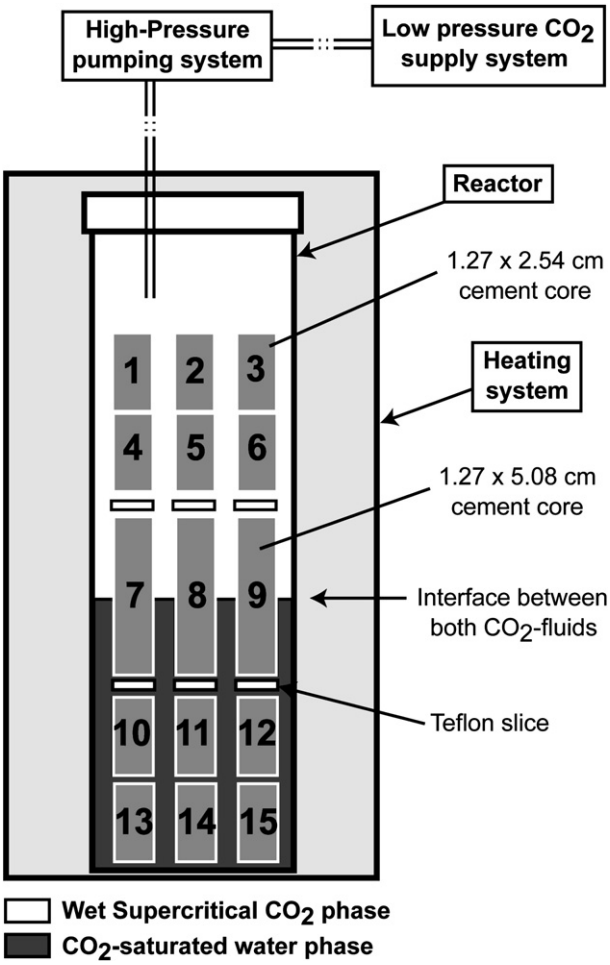

Fig. 1. Simplified scheme showing the CO_2 reactor and the different components of the set-up. The cylindrical samples are immersed in wet supercritical CO_2, in CO_2-saturated water, or at the interface between the two fluids.

cement cubes. Then the cores are cut to about 2.5-cm or 5.0-cm length.

A CO_2 set-up that allows performing controlled and monitored tests under downhole pressure, temperature and fluid-composition conditions, is used. It is composed of a low-pressure CO_2-supply system, a high-pressure pumping system, a reactor with its heating system, and a depressurization system (Fig. 1). A technical description of the equipment and the procedure used to perform CO_2 experiments is presented in detail in Barlet-Gouédard et al. (2006; 2007) [9,10]. The typical set-up is designed to get a quick overview of the behavior of cement with two CO_2 fluids. It aims at obtaining data simultaneously from CO_2-saturated water (lower part of the reactor), wet supercritical CO_2 (upper part of the reactor), and the interface between the two CO_2 fluids.

The open reactor is loaded with the cement samples, and the required amount of liquid fluid (water or brine) is added until the fluid has reached the middle of the samples placed on the second level (Fig. 1). Then the reactor is closed and the heating device is set in place. Heat and CO_2 pressure are applied and increased regularly in order to reach final temperature and pressure in about 2 h. Temperature and pressure are monitored and maintained constant for the duration of the test (from a few hours to several months). At the end of the test period, the heaters and the pumping system are stopped. Temperature and consequently pressure slowly decrease. When the temperature falls to 55 °C, the pressure-release system is activated. It is adjusted to continuously and smoothly release pressure over a few hours. The overall cooling down and pressure-release process lasts approximately 10 h to avoid any damage to the cement samples.

The CO_2 experiments are performed under static conditions, i.e. without stirring in the vessel. These conditions are considered as a realistic simulation of the CO_2-exposure conditions at the formation/cement sheath interface (the exposure may occur under a dynamic state during CO_2 injection only around the perforations). Water is used rather than saline solution to provide more extreme conditions, as CO_2 is highly soluble in pure water [12]. The test conditions are fixed to 90°C and 280 bars for all experiments. These conditions are in the range of specifications for CO_2-storage applications (Fig. 2). The tests are performed at different durations: half-day (13 h), two days (44 h), four days (88 h), one week (188 h), three weeks (523 h), six weeks (1006 h), three months (2033 h) and six months (4410 h). For each experiment, the volume content of the CO_2 fluids in the reactor is about 40% water and 60% CO_2 at atmospheric pressure and room temperature. At 90°C and 280 bars, water is a liquid fluid whereas CO_2 is in its supercritical state [13–15]. For these conditions, the water mole fraction in the supercritical CO_2 phase is about 1.8%, the CO_2 mole fraction in water is 2.25% [16], and pH of the CO_2-saturated water phase reaches low values of about 3 [17].

The characteristics of the CO_2-related alteration of Portland cement with time, detected in measuring the thickness of the alteration front and in analyzing mineralogical changes by X-ray diffraction, are presented in the following section.

3. Sample characterization at the macroscopic scale

Carbonation features are observed already after a few days of CO_2 exposure in both the wet supercritical-CO_2 phase and CO_2-saturated water phase (Fig. 3). Carbonation of Portland cement is achieved as follow; the dissolution of CO_2 in pure water produces carbonic acid. Aqueous CO_2 species react with calcium hydroxide from Portland cement (portlandite) to form calcium carbonate and water (1).

$$Ca(OH)_2 + H^+ + HCO_3^- \rightarrow CaCO_3 + 2H_2O. \quad (1)$$

It also reacts with the calcium silicate hydrates (C–S–H) of cement to form calcium carbonate and a silica gel (2) [18–24].

$$C\text{–}S\text{–}H + H^+ + HCO_3^- \rightarrow CaCO_3 + SiO_2, nH_2O \text{ (silica gel)}. \quad (2)$$

Furthermore, as CO_2 is in excess in the reactor, the newly formed calcium carbonate may partly dissolve in the presence of carbonic acid to form water-soluble calcium bicarbonate (3)

$$CaCO_3 + H^+ + HCO_3^- \rightarrow Ca(HCO_3)_2 \quad (3)$$

that may also react with more calcium hydroxide to form new calcium carbonates and fresh water available in the matrix (4) [18,19].

$$Ca(HCO_3)_2 + Ca(OH)_2 \rightarrow 2CaCO_3 + 2H_2O. \quad (4)$$

After the first days of CO_2 exposure, millimeter-size calcium carbonate grains have precipitated onto the surface of the samples

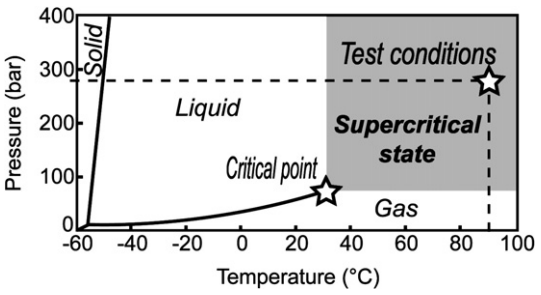

Fig. 2. Phase diagram for CO_2 (modified after Hollister, 1981 [13]). The critical point for CO_2 (T=31.6 °C and P=73 bars) and the experimental conditions of this study (T=90 °C and P=280 bars) are shown with empty stars.

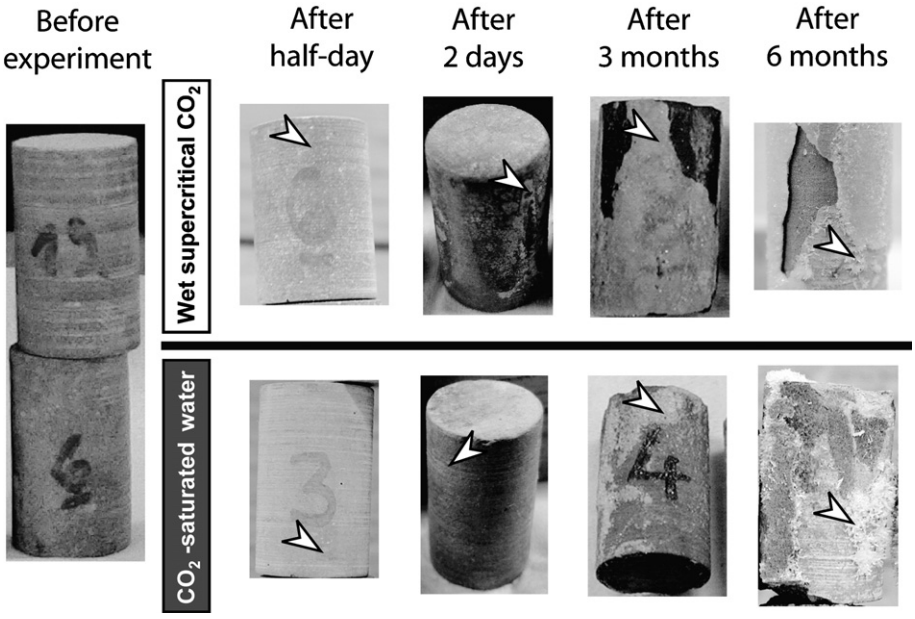

Fig. 3. Portland cement samples before CO_2 exposure and after several selected durations of experiment in CO_2-fluids at 90 °C and 280 bars. White arrows indicate calcium carbonate precipitation at the surface of the cement cores. The samples underwent a strong degradation after three and six months in CO_2.

(Fig. 3). After three and six months, the samples exhibit a thick calcium carbonate layer, and the sample carbonation is commonly accompanied by the formation of cracks. As expected [25,26], the pH of water equilibrated with cement cores has dropped from an initial value of 13 down to 6–7 after CO_2 exposure. When cutting the samples along their axial plane (Fig. 4), a brownish corona is observed at the edge of the samples, already after the first days of CO_2 attack. This brownish concentric zone strongly differs from the greyish inner part of the samples. The thickness of this alteration front increases with exposure time from about 0.5–1 mm after a half-day, 1–2 mm after two days to 5–6 mm after three weeks of attack. After six weeks, the front (about 7 mm) has reached the central part of the samples.

For mineral-phase identification in the different zones of the samples, pieces (10 to 50 mg) were extracted from the edge and the centre of the samples, at different durations of CO_2 attack up to six months. Then the sample pieces were ground for powder X-ray diffraction analyses with a D5000 SIEMENS diffractometer. The starting cement is mainly composed of portlandite, anhydrous calcium silicate (C_2S, C_3S) and calcium silicate hydrates (C–S–H) (Fig. 5). After a half-day (13 h) in wet supercritical CO_2, the diffraction of the sample edge shows the occurrence of two calcium carbonate polymorphs: abundant calcite and traces of aragonite. Vaterite was not detected. In this outer zone, portlandite and calcium silicate phases have completely reacted with CO_2 to form calcium carbonate polymorphs. In the centre of the sample, portlandite and C_2S still occur but are less abundant than before the attack. Furthermore, some calcium silicate phases (C_3S) occur as relict and traces of calcite are detected. Therefore, carbonation and CO_2-related chemical changes are not limited to the rim of the samples. After four days of experiment, the edge of the cement sample is made of calcite and

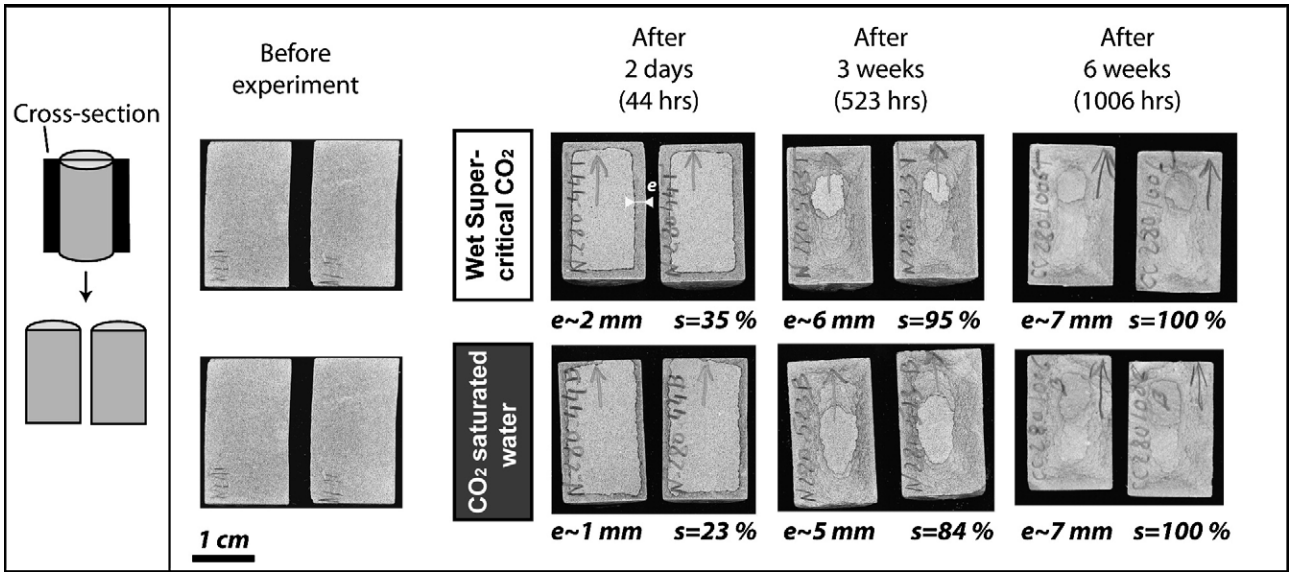

Fig. 4. Cross-sections of the Portland cement cores before attack and at different selected durations of experiment at T=90 °C and P=280 bars, according to the fluid type in which the samples are placed in the reactor. e: thickness of the alteration front; s: ratio between the alteration front surface and the whole cross-section surface.

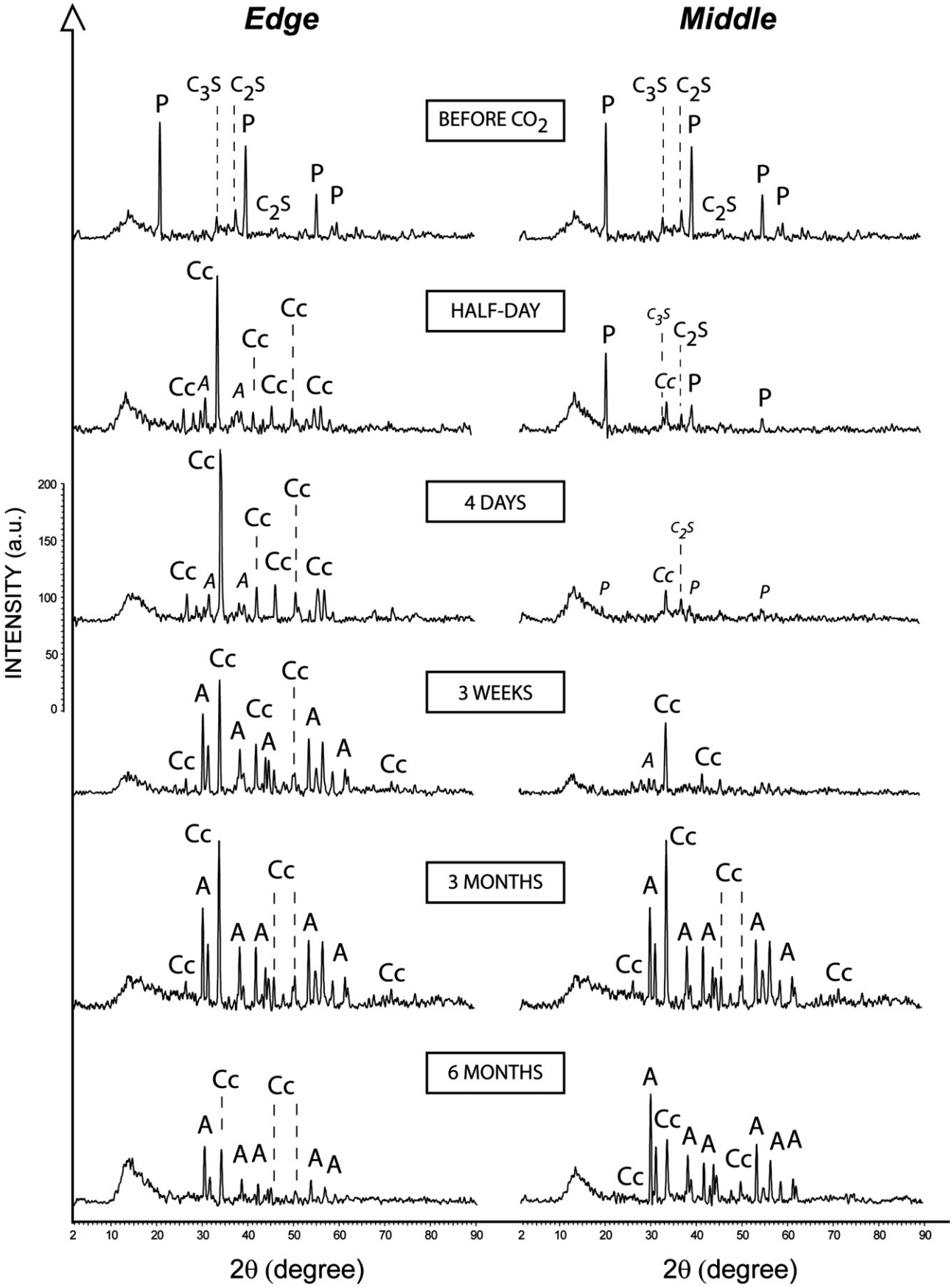

Fig. 5. X-ray diffraction analyses on Portland cement (at the edge and at the core of the samples) before attack and at different durations of experiment up to six months at T=90 °C and P=280 bars in wet supercritical CO_2. Abbreviations: P, Portlandite; *P*, Portlandite relict; Cc, Abundant calcite; *Cc*, low amount of calcite; A, Aragonite; *A*, low amount of aragonite; C_3S and C_2S, abundant calcium silicate; *C_3S* and *C_2S*, calcium silicate relicts.

aragonite, whereas its central part exhibits calcium silicate phases, relicts of portlandite, and slightly more calcite than after a half-day. After three weeks in CO_2 fluids, the edge of the sample has the same mineralogical composition as the one obtained after four days of exposure. However, the central part of the sample contains neither portlandite nor calcium silicate phases. All the Portland cement components have reacted to form calcium carbonates. It should be noted that amorphous components as silica gel cannot be identified from X-ray diffraction only. Finally, after three and six months of experiment, aragonite and calcite abundantly occur through the whole sample (Fig. 5).

Therefore, sample characterization shows that the penetration of the alteration front through the cement attests to a rapid and effective process. The alteration starts from the edge and proceeds towards the centre to produce a chemically heterogeneous sample. However, carbonation is not restricted to that growing alteration zone since the inner part of the sample is found to react within the first hours of experiment, as attested by sporadic calcium carbonate occurrence.

The effect of CO_2 on cement integrity requires a complementary study of the alteration process at the micrometer scale. Further sample characterization using the scanning electron microscopy (SEM) is presented in the following section.

4. Characterization at the micrometer scale using the SEM

Polished thin sections of cement samples are used for SEM (Hitachi S3400 model) analyses and back-scattered electron (BSE) images (Fig. 6). This microscopic approach shows a clear heterogeneous alteration pattern, even after the first days of exposure [9,10,27]. Alteration is characterized by a series of carbonation and dissolution fronts, which progressively translate with time from the rim towards the core of the cement samples. This geometry of distinct concentric zones is observed at all test durations. From the rim towards the core, the altered cement consists of a carbonated zone, a carbonation front, a dissolution front and the inner part of sample. The carbonated zone contains calcium carbonate, silica gel and calcium-depleted calcium silicate phases. Ahead of this zone, the carbonation front is a thin layer (50 to 200 μm wide) of very low porosity, in which abundant calcium carbonates have precipitated. The carbonation front contrasts with the dissolution front, which is a zone of high porosity where Portland cement phases (portlandite and calcium silicate hydrate phases) progressively dissolve to form calcium carbonates backwards, in the carbonation front. Indeed, dissolution of the cement hydration products provides OH^- and Ca^{2+} ions towards the carbonated area [28]. Finally, the inner part of the sample corresponds to the internal part of the cement still containing portlandite, anhydrous calcium silicate still not hydrated, and a very low amount of calcite precipitation, as identified by X-ray analyses (Fig. 5). Such an alteration pattern has also been recently described from experiments performed on conventional cement with a static volume of brine subject to high CO_2 pressure [29].

For longer CO_2 exposures (e.g. three months), this particular geometry of concentric reaction fronts is translated towards the central part of the samples, and relicts of these fronts are commonly observed backwards in the carbonated zone (Fig. 7a). These “paleofronts” are made of zones with low amounts of silica gel and well-crystallized calcium carbonate, intercalated by silica gel-rich zones that contain only micrometer-scale calcium carbonate nodules (Fig. 7b). This complex series of paleofronts corresponds to discontinuities through the sample and may play a crucial role in the mechanical weakening of Portland cement.

Therefore, as observed on SEM-BSE images, the carbonation and dissolution fronts indicate that the porosity of Portland cement is affected by the reactions of cement components with CO_2. Water-permeability measurements were performed on the cement samples before and after different durations of CO_2 exposure. The flow of water is measured with an effective confining pressure of 28 bars and a differential pressure of 35 bars. This measurement method did not allow detection of any change due to the CO_2 attack, as the permeability always remained below the detection limit of 8 μDarcy. Two other methods were chosen to quantify the evolution of the porosity and the pore-entrance size distribution: mercury intrusion porosimetry and BSE image analysis.

5. Quantification of the evolution of cement porosity

In a first stage, the evolution of the cement porous network with time can be estimated by mercury-intrusion porosimetry (MIP)

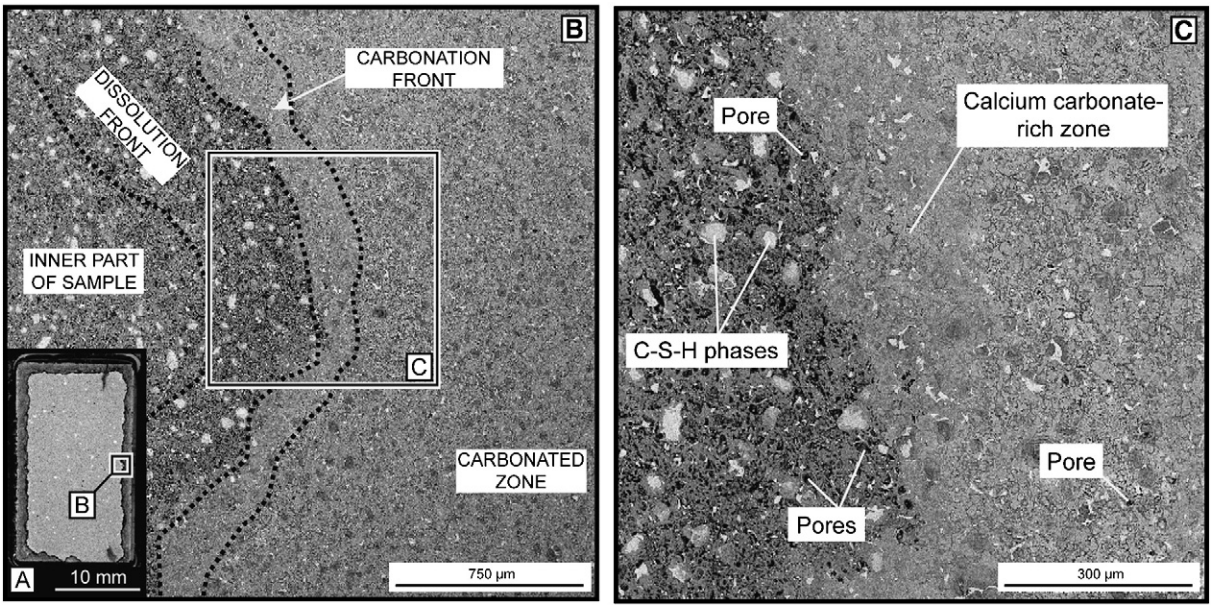

Fig. 6. (A) Cross-section of a Portland cement sample immersed in CO_2-saturated water during two days at 280 bars and 90 °C. Back-scattered electron images show the different zones in the sample. The concentric alteration front is clearly visible. (B, C) The low-porosity carbonation front and the high-porosity dissolution front occur as chemical reaction fronts. Fronts have been marked by dashed lines on the left picture.

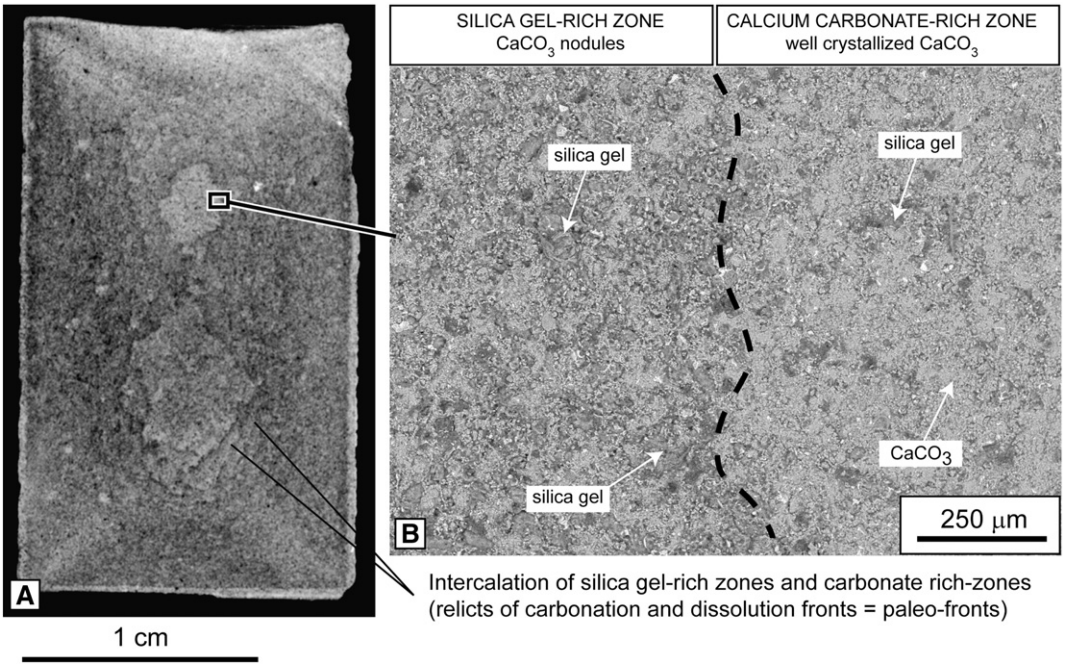

Fig. 7. Polished cross-section (A) and BSE image (B) of a Portland cement sample tested during six months at 280 bars and 90 °C in wet supercritical CO_2 fluid.

measurements on the samples exposed either to wet supercritical CO_2 or to CO_2-saturated water. This measurement allows quantification of the global porosity of the samples exposed to CO_2.

5.1. Mercury intrusion porosimetry measurements

MIP estimates the pore size over a wide range (theoretically from 0.003 µm to 360 µm). The measurements are carried out by two different laboratories (Micromeritics France; Institut de Physique du Globe in Strasbourg) on 1.25 cm diameter × 2.5 cm length samples. The samples are dried at 100 °C at atmospheric pressure for 60 h to empty the pores of any existing fluid. Then, they are weighed and transferred to the measurement cell. After the air is evacuated, the cell is filled with mercury. Since it is a non-wetting fluid, mercury does not enter into the specimens unless pressure is applied. During the test of mercury intrusion porosimetry, the pressure of intrusion ranges between 0.035 and 2000 bars. The maximum intrusion pressure of 2000 bars corresponds to a minimum pore entrance size of 6.2 nm). The equilibrium time is 20 s. Therefore, the results represent the porosity filled with mercury at 2000 bars, i.e. the volume of cavities

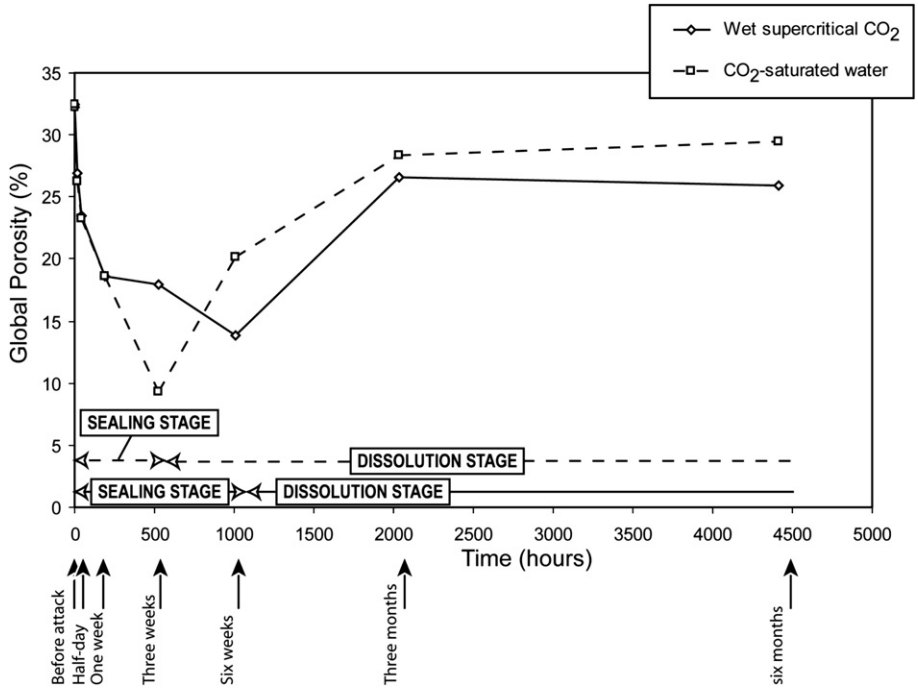

Fig. 8. Evolution of the global porosity deduced from mercury intrusion porosimetry (MIP) measurements in Portland cement core samples exposed to wet supercritical CO_2 and in CO_2-saturated water, at 90 °C under 280 bars, up to six months. Both plugging and dissolution stages are highlighted.

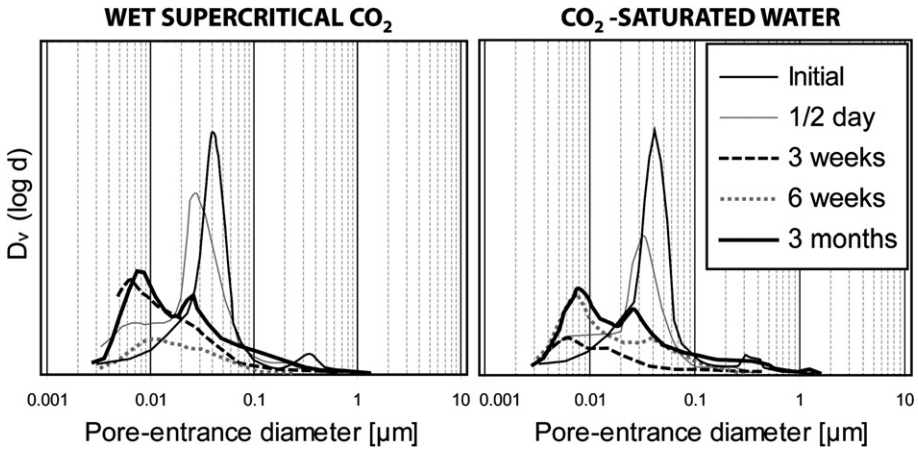

Fig. 9. Evolution of the threshold diameter with time estimated from mercury intrusion porosimetry (MIP) on Portland cement samples exposed to wet supercritical CO_2 and CO_2-saturated water up to three months. See text for explanations.

connected to the surface through a percolative path with a diameter greater than 6.2 nm. Pressure is applied to the mercury in progressive increments, and the corresponding intruded volumes are monitored. Two intrusion–extrusion cycles are performed to determine irreversible and reversible intrusion volumes. After the first intrusion, the pressure restored at the end of the first extrusion equals to the atmospheric pressure. A volume of mercury is thus trapped in the porous network. After the second intrusion, the volume of mercury at the end of the second extrusion is equivalent to the one at the end of the first extrusion. The two curves of mercury extrusion are superimposed, which indicate that the samples did not suffer significant damage during the mercury intrusion.

The initial mercury porosity of Portland cement is 33% (Fig. 8). In wet supercritical CO_2, the porosity continuously decreases from 33% to 15% in the first six weeks. After a decrease from 33% to 27% in the first hours of exposure, the decrease slows down over the next six weeks. Then porosity increases from 15% to 27% between six weeks and three months of exposure. It remains at the same value after six months of CO_2 exposure, slightly below the initial porosity value. In the CO_2-saturated water phase, the porosity also varies following two distinct phases. During the first three weeks, porosity decreases from 33% to 9%. At this stage of CO_2 exposure, the carbonation front has nearly reached the central part of the samples (Fig. 4). Then, from three weeks to three months, the porosity increases from 9% to 28%. After six months, the porosity reaches nearly 30%, slightly lower than the initial porosity value (Fig. 8). Therefore, in both CO_2 fluids, the MIP results show an initial sealing stage related to carbonation of the sample, followed by a dissolution stage. The dissolution stage occurs earlier in CO_2-saturated water than in wet supercritical CO_2, and is limited over time. This limitation over time may be related to the experimental set-up that does not permit fluid renewing. The experiment is a closed system since the ionic transport remains limited over time. The increase of cement porosity is therefore blocked over time.

Since the pores in cement-based material are not cylindrical and not entirely and equally accessible to the outer surface of the sample, it has been claimed that MIP measurements do not provide the pore-size distribution, but only the pore-entrance size distribution [30–33]. Nevertheless, MIP allows to determine a threshold diameter by estimating the volume-log diameter distribution $D_v(\log d)$ [33]. It appears to be a useful index of the percolative steps in the intrusion of mercury under pressure. To the extent that the intrusion process at a specific pressure involves only Darcy flow, the threshold diameter would seem to be a valid comparative parameter, related to permeability in cement-paste systems. The threshold determined during the first mercury intrusion thus correlates indirectly to the permeability of the cement-based system [34].

Fig. 9 represents the evolution of this threshold diameter at several experimental time scales in both CO_2 fluids. Before the experiment, a clear peak corresponding to the threshold diameter is visible at 0.04 µm. A second small peak is located at about 0.3 µm. In wet supercritical CO_2, the threshold diameter decreases from 0.04 µm initially to about 0.03 µm after a half-day of exposure (13 h), and is about 0.01 µm after six weeks of exposure. This is attributed to the

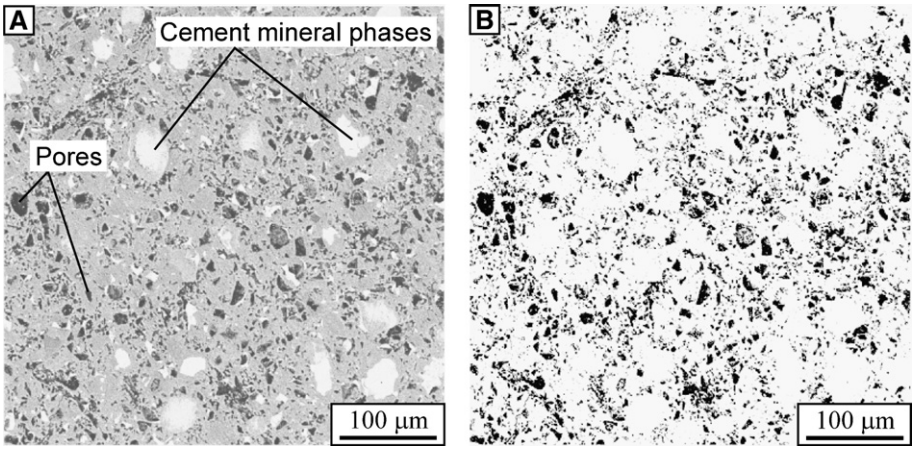

Fig. 10. SEM-BSE image of Portland cement (A) and binarization of the initial grey-level BSE image (B) using the threshold tool of the image software. The proportion of the black part of the binary image is measured using the histogram tool of the image software. The value is considered to correspond to a local 2D porosity.

sealing stage during which calcium carbonate precipitates in the pores. After three months of exposure, the threshold-diameter estimates exhibit two peaks: one is 0.008 μm and one at 0.03 μm. These peaks correspond to a reorganisation of the porous network with a component showing a reopening of the pore entrance. The data at six months roughly superimpose those at three months. A similar trend is observed for the samples placed in CO_2-saturated water, except that the pore-entrance reopening seems to occur earlier (at six weeks) than in wet supercritical CO_2 (at three months). Furthermore, the reopening of the largest pore entrance (0.3–0.4 μm) is visible in the samples tested in CO_2-saturated water, and does not occur in the wet supercritical CO_2 phase.

Therefore, the MIP data show a two-stage evolution of the porous network and its connectivity: a first sealing stage related to porosity plugging by calcium carbonate precipitation, followed by an increase in the porosity and a reopening of the pore-entrance diameter that may be linked to a dissolution phase. The latter seems more efficient in CO_2-saturated water than in wet supercritical CO_2. These MIP measurements are performed on the whole volume of samples. Although they provide information on the global porosity evolution, they do not account for local porosity gradients related to carbonation or dissolution processes though the samples. We present in the following section a method that is used to estimate the relative variation of porosity in heterogeneous samples.

5.2. Local porosity profiles

Local-porosity profiles are generated from SEM-BSE image analyses. The BSE images are 256 grey-level images of the polished section (1 mm-thick) surface (Fig. 10). Each image is a 1024×1024 pixel-square of surface ranging practically from 50×50 to 1000×1000 μm. The grey-levels of BSE images are a function of the

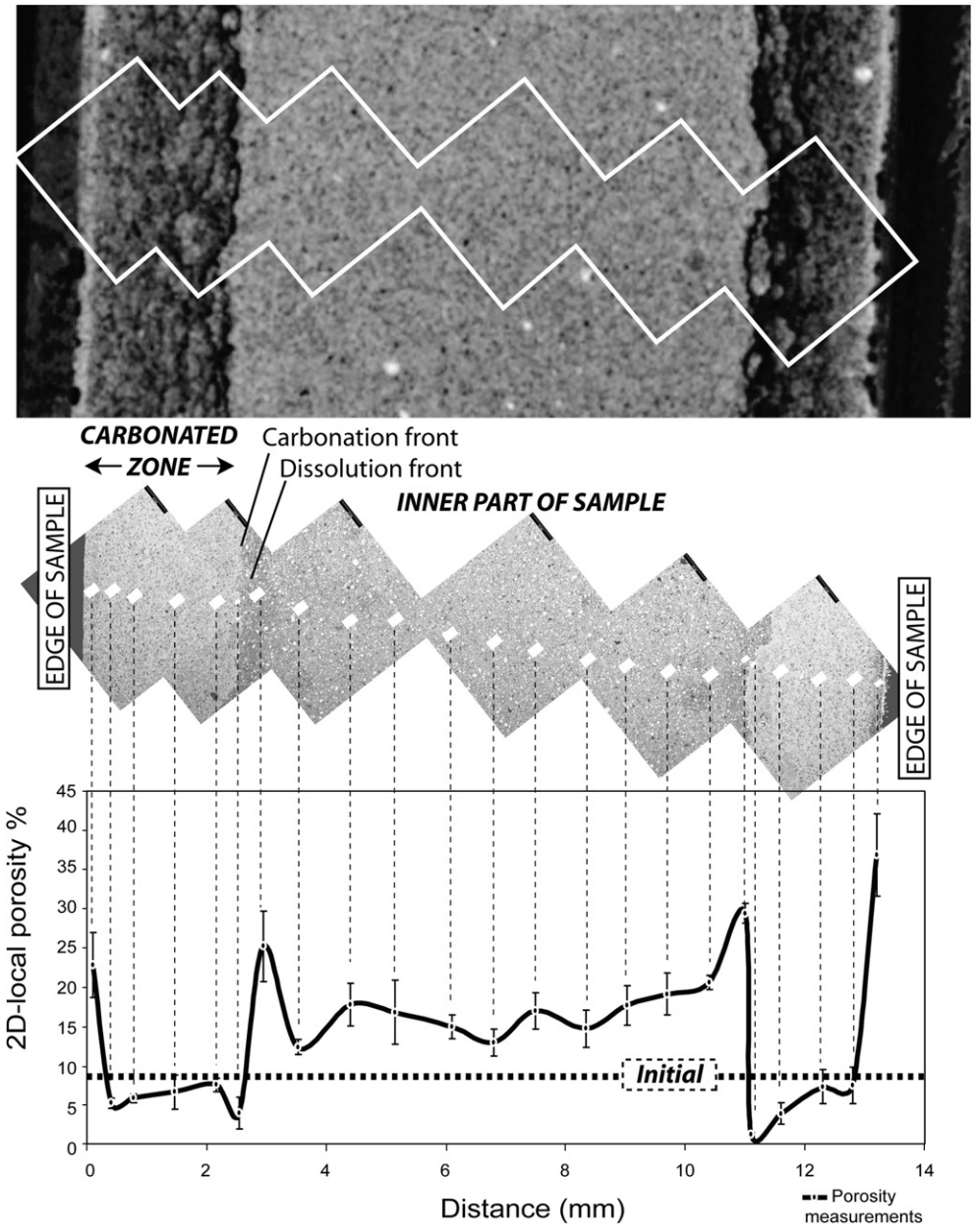

Fig. 11. Polished section (above) and SEM-BSE image profile (middle) through a Portland cement core attacked during four days in CO_2-fluid at 280 bars and 90 °C. The different carbonation and dissolution zones are identified. The white rectangles locate the areas where local porosity was measured by thresholding the BSE images. The results of the local porosity estimates with their error bars along the profile are reported below.

elemental mass of the scanned material; therefore, the BSE device detects the lowest mass part of the surface. These lowest mass surfaces that appear on the BSE image as the darkest grey-levels correspond to holes or to the epoxy used to make the thin section, filling the porosity of the sample. Using Adobe Photoshop image software, the image is binarized by thresholding the grey-level scale to a value that gives the best fit of the black parts of the initial image. The proportion of the black part of the binary image is measured using the histogram tool of the image software. The value is then considered to correspond to the porosity [30,35]. The repeatability of this method is checked by at least three porosity measurements on the same selected zone estimating the averaged local porosity and the standard deviation for each measurement. Furthermore, two sandstones with porosities of 10% and 20% (estimated by standard porosity methods) were used as standard rocks to control the efficiency of this method. The SEM-BSE image treatment of polished thin sections of these sandstones estimated the same values of 10% and 20%. 500×500 µm-square BSE images are taken for porosity estimates. With this magnification, the method gives good constraints for pore sizes greater than 1 µm. This pore scale differs from that of MIP measurements, which provided information on the pore-entrance size up to 6 nm. Furthermore, the estimate is a two-dimensional porosity corresponding to a relative porosity. It is comparable between samples that underwent different durations of CO_2 exposure, but is not an absolute porosity value.

Before CO_2 exposure, the local porosity of Portland cement is estimated with several BSE images. The average local porosity is 8 ± 1%. For a precise quantification of the local porosity through the core samples, profiles were generated for samples attacked at different durations. For instance, Fig. 11 shows a local-porosity profile through a sample exposed for four days. Porosity drastically varies from the edge to the middle of the sample. The sample rim is made of a very thin zone with high porosity values (20 to 40%). This high-porosity region is a zone of mechanical damage predating CO_2 attack and due to the coring of the cement. Then, porosity decreases to 5–8% in the carbonated zone that contains calcium carbonate, silica gel and calcium-depleted calcium silicate hydrous phases. In the thin calcium carbonate-rich carbonation front (~100-µm wide), porosity shows the lowest values (below 5%). Then, the dissolution front is marked by a high porosity (25 to 30%). This front is a very reactive area in which Portland cement components progressively dissolve to form calcium carbonate backwards from the carbonation front.

Finally, porosity decreases to a value around 15% in the inner part of sample. This average value is higher than the porosity value for an unattacked sample (8%). This method therefore confirms that the inner part of sample is not a sound zone. A dissolution process affected the inner part of sample in the first days of attack. This process was already detected with X-ray analyses showing that CO_2-related alteration of Portland cement is not restricted to the alteration front in the first hours of CO_2 exposure. The central part of the sample also reacts with CO_2.

The evolution of local-porosity profiles with time is shown in Fig. 12 (up to six months). In both CO_2 fluids, the translation of the carbonation front and nearby dissolution front with time towards the center of the Portland cement samples is well observed from a half-day to three weeks of CO_2 exposure. Even after a half-day of exposure the porosity of the inner part of the sample has increased from 8% (initial porosity) to 25% in the wet supercritical CO_2 phase and from 8% to 15% in CO_2-dissolved water. From a half-day to three weeks of exposure, the porosity of the inner part of sample decreases in both fluids and reaches the values for an unattacked sample (about 8%). This decrease can be related to calcium carbonates precipitating in the pores of the cement paste. In contrast, after three months and six months, no carbonation front is visible since it has reached the center of the sample, and the local-porosity profile shows a clear increase of porosity compared to the effects after three weeks (from about 8% to 15–20%). This porosity increase may come from the dissolution of the newly formed calcium carbonate, when portlandite and C–S–H phases

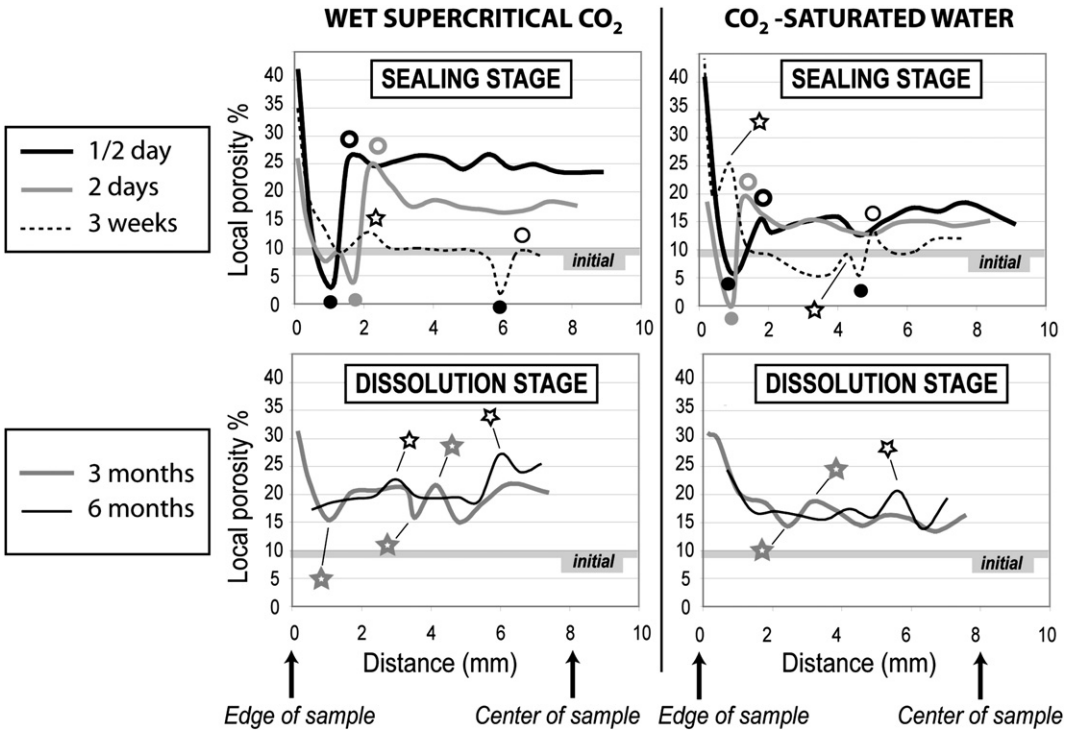

Fig. 12. Evolution of the local porosity profiles with time from the edge to the core of the samples exposed either in wet supercritical CO_2 or in CO_2-saturated water, during a half-day, two days, three weeks, three months and six months at 280 bars and 90 °C. The gray dashed line marks the initial local porosity (for an unattacked sample). Full circle: carbonation front; empty circle: dissolution front; star: paleofront.

have completely reacted with CO_2. At this stage, the samples being mainly made of calcium carbonate and silica gel, since CO_2 is in excess in the reactor, dissolution of the newly formed calcium carbonate is more likely to be responsible for this porosity increase. On the three-week, the three-month and the six-month porosity profiles, the local porosity becomes more variable than for the tests at shorter duration, depicting a complex pattern within the cement cores. As highlighted above, some relicts of carbonation and dissolution fronts (the so-called "paleofronts") are observed within the carbonated zone (Fig. 7). They originate from the advancing fronts towards the center of the cement sample. This series of paleofronts of carbonation and dissolution are responsible for such local variations of the cement porosity (Fig. 12: e.g. porosity peak at ~1 mm on the three-week profile in CO_2-saturated water).

Therefore the local-porosity profiles show a two-stage evolution of Portland cement porosity, similar to that deduced from MIP data: a first sealing stage related to a porosity plugging by calcium-carbonate precipitation, followed by an increase of the porosity corresponding to a dissolution phase. Furthermore, they provide information on the local porosity gradients through the cement samples highlighting the series of fronts (carbonation front, dissolution front, paleofronts…) that are well-marked discontinuities in the cement samples.

6. Discussion

The use of the two types of porosity measurements described above yields information on the evolution of the porous network of the samples exposed to wet supercritical CO_2 and CO_2-saturated water. On one hand, the MIP data permit quantifying the evolution of the global porosity of the samples; on the other hand, the SEM-BSE image analysis highlights some sharp local porosity gradients related to carbonation or dissolution processes across the altered samples. The results obtained from both methods show that the cement porous network and its connectivity underwent a two-stage evolution: (1) a sealing stage related to a porosity plugging by calcium carbonate precipitation, and (2) a reopening of the pore-entrance diameter that may be linked to a dissolution phase; the latter being more efficient in CO_2-saturated water than in wet supercritical CO_2.

CO_2 alteration of Portland cement is a rapid process. Already after a half-day under simulated downhole conditions a millimetre-scale alteration front is visible, and after six weeks of CO_2 exposure it has reached the center of the samples. This alteration process is characterized by a heterogeneous pattern made of a series of carbonation/dissolution fronts and relicts of these fronts (paleofronts). The relative-porosity profiles quantified by SEM-BSE image analysis show that these fronts mark chemical and physical discontinuities across the samples. Furthermore, this method, coupled with the X-ray diffraction analyses, shows that the inner part of the samples is not a sound zone: it has already rapidly reacted in the first days of exposure, as seen by an increase of the local porosity and sporadic calcite precipitation. Therefore, the CO_2 alteration of cement is not restricted to the alteration front.

These experimental results differ from other studies conducted by Jacquemet et al. [36] and Kutchko et al. [29] who showed a slower and limited penetration of CO_2 with time. On one hand, the pressure and temperature conditions of their experiments are different from those in the present study. On the other hand, they used a static volume of brine subject to supercritical CO_2 rather than pure water subject to supercritical CO_2. Thus, the CO_2 solubility in their experiments is far lower than in our simulations. This lower CO_2 solubility may substantially limit the kinetics of cement alteration, because far less CO_2 is available in the system to react with cement. Finally, these experimental studies are performed without continuously flowing CO_2 fluids through the cement sample. This may also limit the degradation and loss of structural integrity of cement observed by Duguid et al. who indeed conducted experiments with flux of acidic brine [37]. Thus, the use of a continuous CO_2-saturated water flux through Portland cement may accelerate its degradation under wellbore pressure and temperature conditions.

It is noteworthy that the laboratory experiments on CO_2-related cement degradation are simulations that really need to be thoroughly compared to field data. A study of one cement sample recovered from a well located in the CO_2 enhanced oil recovery field (SACROC unit) in the Permian basin of West Texas was recently conducted [4]. The sample was retrieved from a 55 year-old well with 30 years of CO_2 exposure as both an injector and a produced at the unit. The sample, located about 3 m above the contact with the reservoir, showed evidence for CO_2 migration along the casing/cement and cement/shale interfaces. The cement was heavily carbonated to an assemblage of calcite, aragonite, vaterite, and was transformed to a distinctive orange zone, very similar to the alteration front described here. All the measurements for this single well, show significant carbonate mineralization over a period of 30 years. However, these authors were unable to quantify the amount of CO_2 migration that occurred along cement/casing and cement/shale cap-rock interfaces. The quality of these interfaces appears to be the most critical issue in the performance of wellbore systems in a CO_2-storage reservoir. Further experiments simulating the cement/casing and cement/rock interfaces in CO_2-rich environment clearly need to be conducted.

7. Conclusions

The experimental methodology and microscopic study reported in this paper highlight the extent of cement modification in response to CO_2 fluids under simulated downhole conditions. CO_2-related alteration of Portland cement is characterized by a complex series of concentric fronts (carbonation and dissolution fronts, relicts of these fronts…) in both CO_2 fluids. This chemical alteration is a very effective process. The evolution of the global porous network can be estimated by mercury intrusion porosimetry. In concert with these measurements, BSE image analysis allows quantification of the local porosity gradients encountered through the samples exposed to CO_2. Both methods show an initial sealing stage related to precipitation of calcium carbonate that plugs the porosity, followed by a dissolution stage marked by a significant increase of porosity. It is emphasized that carbonation of Portland cement is not a continuous process that plugs the porosity. These results show a rapid and extensive degradation of Portland cement in the presence of CO_2. Guaranteeing well integrity for carbon storage applications requires development of CO_2-resistant materials that will be used for primary cementing of new CO_2-injection wells, as well as for repairing operations. Materials for plug and abandonment operations also must be characterized with respect to their long-term durability under CO_2 environment.

Acknowledgements

The authors would like to thank the management of Schlumberger for permission to publish this paper. The laboratory staff of Schlumberger Riboud Product Center, especially Yamina Boubeguira and Hafida Achtal, is gratefully acknowledged. The authors also would like to thank the technical staff of the Laboratoire de Géologie at the Ecole Normale Supérieure, especially Guy Marolleau for experimental advices and Roland Caron for sample cross-sections preparation. An anonymous reviewer is acknowledged for fruitful comments and suggestions that contributed to improve the first version of the manuscript.

References

[1] M.T. Power, M.A. Leicht, K.L. Barnett, Converting Wells in a Mature West Texas Field for CO_2 Injection, Paper SPE 20099, 1989.
[2] G.J. Mizenko, North Cross (Devonian) Unit CO_2 Flood: Status Report, Paper SPE/DOE 24210, 1992.

[3] J.K. McDaniel Branting, D.L. Whitman, The Feasibility of Using CO_2 EOR Techniques in the Powder River Basin of Wyoming, Paper SPE 24337, Casper, Wyoming, 1992.
[4] J.W. Carey, M. Wigand, S. Chipera, et al., Analysis and performance of oil well cement with 30 years of CO_2 exposure from the SACROC unit, West Texas, USA, International Journal of Greenhouse Gas Control (2007) 75–85. doi:10.1016/S1750-5836(06)00004-1.
[5] S. Bachu, Sequestration of CO_2 in geological media: criteria and approach for site selection in response to climate change, Energy Conversion and Management 41 (9) (2000) 953–970.
[6] Y.F. Houst, F.H. Wittmann, Depth profiles of carbonates formed during natural carbonation, Cement and Concrete Research 32 (2002) 1923–1930.
[7] M. Thiery, G. Villain, P. Dangla, G. Platret, Investigation of the carbonation front shape on cementitious materials: effects of the chemical kinetics, Cement and Concrete Research 37 (7) (2007) 1047–1058.
[8] G. Villain, M. Thiery, G. Platret, Measurement methods of carbonation profiles in concrete: thermogravimetry, chemical analysis and gamma densimetry, Cement and Concrete Research 37 (8) (2007) 1182–1192.
[9] V. Barlet-Gouédard, G. Rimmelé, B. Goffé, O. Porcherie, Mitigation strategies for the risk of CO_2 migration through wellbores, IADC/SPE 98924, Miami, USA, February, 2006.
[10] V. Barlet-Gouédard, G. Rimmelé, B. Goffé, O. Porcherie, Well technologies for CO_2 geological storage: CO_2-resistant cement, Oil and Gas Science and Technology — Rev IFP 62 (3) (2007) 1–12.
[11] E. Nelson, D. Guillot, Well Cementing, second edition, Schlumberger edition, 2006.
[12] N. Spycher, K. Pruess, CO_2-H_2O mixtures in the geological sequestration of CO_2. II. Partitioning in chloride brines at 12–100 °C and up to 600 bar, Geochimica et Cosmochimica Acta 69 (13) (2005) 3309–3320.
[13] L.S. Hollister, Information intrinsically available from fluid inclusions, in fluid inclusions: applications to petrology, in: Hollister, Crawford (Eds.), Mineral association of Canada, Short course handbook, vol. 6, 1981, pp. 1–12.
[14] J.G. Blencoe, M.T. Naney, L.M. Anovitz, The CO_2–H_2O system: III. A new experimental method for determining liquid-vapor equilibria at high subcritical temperatures, American Mineralogist 86 (2001) 1000–1111.
[15] J.G. Blencoe, The CO_2–H_2O system: IV. Empirical, isothermal equations for re1presenting vapor-liquid equilibria at 110–350 °C , $P \leq 150$ MPa, American Mineralogist 89 (2004) 1447–1455.
[16] N. Spycher, K. Pruess, J. Ennis-King, CO_2–H_2O mixtures in the geological sequestration of CO_2. I. Assessment and calculation of mutual solubilities from 12 to 100 °C and up to 600 bar, Geochimica et Cosmochimica Acta 67 (16) (2003) 3015–3031.
[17] K.L. Toews, R.M. Shroll, C.M. Wai, pH-defining equilibrium between water and supercritical CO_2. Influence on SFE of organics and metal chelates, Analytical Chemistry 67 (1995) 4040–4043.
[18] D.D. Onan, Effects of supercritical carbon dioxide on well cements, SPE 12593, Permian Basin Oil & gas recovery Conference, Midland, TX, March 8–9, 1984.
[19] R.A. Bruckdorfer, Carbon dioxide corrosion in oilwell cements, SPE 15176 Billings, MT, May 19–21, 1986.
[20] Z. Sauman, Carbonation of porous concrete and its main binding components, Cement and Concrete Research 1 (1971) 645–662.
[21] T. Baird, A.G. Cairns-Smith, D.S. Snell, Morphology and CO_2 uptake in tobermorite gel, Journal of Colloid Interface Science 50 (2) (1975) 387–391.
[22] A.M. Dunster, An investigation of the carbonation of cement paste using trimethylsilylation, Advances in Cement Research 2 (7) (1989) 99–106.
[23] G.W. Groves, A. Brough, I.G. Richardson, C.M. Dobson, Progressive changes in the structure of hardened C3S cement pastes due to carbonation, Journal of American Ceramic Society 74 (11) (1991) 2891–2896.
[24] K. Kobayashi, K. Suzuki, Y. Uno, Carbonation of concrete structures and decomposition of C–S–H, Cement and Concrete Research 24 (1994) 55–61.
[25] T. Van Gerven, D. Van Baelen, V. Dutré, C. Vandecasteele, Influence of carbonation and carbonation methods on leaching of metals from mortars, Cement and Concrete Research 34 (2004) 149–156.
[26] T. Van Gerven, J. Moors, V. Dutré, C. Vandecasteele, Effect of CO_2 on leaching from a cement-stabilized MSWI fly ash, Cement and Concrete Research 34 (2004) 1103–1109.
[27] G. Rimmelé, O. Porcherie, V. Barlet-Gouédard, B. Goffé, Quantifying CO_2-related alteration of Portland cement: experimental approach and microscopic methodology, Wellbore Integrity network Meeting, Princeton, N.J, USA, March 29, 2006.
[28] B. Bary, A. Sellier, Coupled moisture-carbon dioxide-calcium transfer model for carbonation of concrete, Cement and Concrete Research 34 (10) (2004) 1859–1872.
[29] B. Kutchko, B. Strazisar, D. Dzombak, G. Lowry, Degradation of well cements under geologic sequestration conditions, Wellbore Integrity network Meeting, Princeton, N.J, March 29, 2006.
[30] S. Diamond, Mercury porosimetry. An inappropriate method for the measurement of pore size distributions in cement-based materials, Cement and Concrete Research 30 (2000) 1517–1525.
[31] S. Chatterji, A discussion of the paper "Mercury porosimetry. An inappropriate method for the measurement of pore size distributions in cement-based materials", Cement and Concrete Research 31 (2001) 1657–1658.
[32] S. Wild, A discussion of the paper "Mercury porosimetry. An inappropriate method for the measurement of pore size distributions in cement-based materials", Cement and Concrete Research 31 (2001) 1653–1654.
[33] F. Moro, H. Böhni, Ink-bottle effect in mercury intrusion porosimetry of cement based materials, Journal of Colloid and Interface Science 246 (2002) 135–149.
[34] Z. Liu, D. Winslow, Sub-distributions of pore-size: A new approach to correlate pore structure with permeability, Cement and Concrete Research 25 (1995) 769–778.
[35] N.K. Tovey, M.W. Hounslow, Quantitative micro-porosity and orientation analysis in soils and sediments, Journal of the Geological Society (London) 152 (1995) 119–129.
[36] N. Jacquemet, J. Pironon, E. Caroli, A new experimental procedure for simulation of H_2S+CO_2 geological storage — application to well cement aging, Oil and Gas Science and Technology — Rev IFP 60 (1) (2005) 93–206.
[37] A. Duguid, M. Radonjic, G. Scherer, The effect of carbonated brine on the interface between well cement and geologic formations under diffusion-controlled conditions, 8th International conference on Greenhouse Gas Control Technologies, Trondheim, Norway, June 19–22, 2006.